AD-A129 367 TRANSONIC NOISE GENERATION BY DUCT AND PROFILE FLOW(U) 1/1
MAX-PLANCK-INST FUER STROEMUNGSFORSCHUNG GOETTINGEN
(GERMANY F R) G E MEIER ET AL. APR 83 DAJA37-81-C-0251

UNCLASSIFIED F/G 20/1 NL

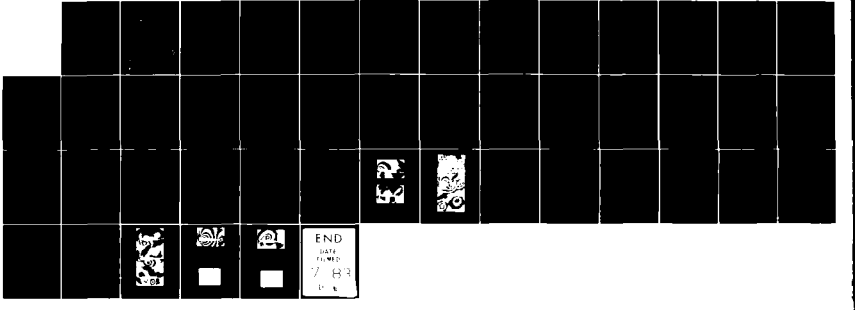

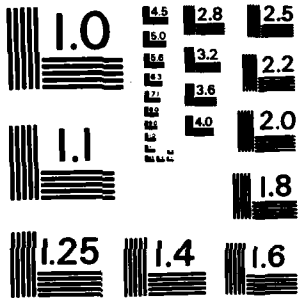


MICROCOPY RESOLUTION TEST CHART
NATIONAL BUREAU OF STANDARDS-1963-A

# TRANSONIC NOISE GENERATION BY DUCT AND PROFILE FLOW

R&D 3037-AN

[redacted] Second Annual Technical Report

by

Dr. G.E.A. Meier

Dipl. Phys. R. Timm

Dr. F. Becker

April 1983

United States Army

EUROPEAN RESEARCH OFFICE OF THE U.S. Army.

London/England

CONTRACT NUMBER DAJA 37-81-C-0251



Contractor: Prof. Dr. E.-A. Müller
MPI für Strömungsforschung
D-3400 Göttingen, Böttingerstr. 4-8

UNCLASSIFIED
SECURITY CLASSIFICATION OF THIS PAGE (When Data Entered)

R&D 3037-AN

| REPORT DOCUMENTATION PAGE | READ INSTRUCTIONS BEFORE COMPLETING FORM |
|---|---|
| 1. REPORT NUMBER | 2. GOVT ACCESSION NO. AD-A129367 | 3. RECIPIENT'S CATALOG NUMBER |
| 4. TITLE (and Subtitle) Transonic Noise Generation by Duct and Profile Flow | 5. TYPE OF REPORT & PERIOD COVERED 2nd Annual Report April 1982 - April 1983 |
| | 6. PERFORMING ORG. REPORT NUMBER |
| 7. AUTHOR(s) Dr. G.E.A. Meier; Dipl. Phys. R. Timm; Dr. F. Becker | 8. CONTRACT OR GRANT NUMBER(s) DAJA 37-81-C-0251 |
| 9. PERFORMING ORGANIZATION NAME AND ADDRESS MPI für Strömungsforschung D-3400 Göttingen Böttingerstr. 4-8 | 10. PROGRAM ELEMENT, PROJECT, TASK AREA & WORK UNIT NUMBERS 6.11.02A 1T16 1102BH57-06 |
| 11. CONTROLLING OFFICE NAME AND ADDRESS USARDSG-UK Box 65, FPO New York 09510 | 12. REPORT DATE April 1983 |
| | 13. NUMBER OF PAGES 41 |
| 14. MONITORING AGENCY NAME & ADDRESS(if different from Controlling Office) | 15. SECURITY CLASS. (of this report) Unclassified |
| | 15a. DECLASSIFICATION/DOWNGRADING SCHEDULE |

16. DISTRIBUTION STATEMENT (of this Report)

Approved for public release; distribution unlimited

17. DISTRIBUTION STATEMENT (of the abstract entered in Block 20, if different from Report)

18. SUPPLEMENTARY NOTES

19. KEY WORDS (Continue on reverse side if necessary and identify by block number)

transonic noise generation, vortex profile flow interaction, transonic flow, digital interferogram analysis

20. ABSTRACT (Continue on reverse side if necessary and identify by block number)

To study the strong sound generation in the case of helicopter rotor vortex interaction, a vortex profile flow interaction experiment is performed in a transonic duct. Vortices are generated upstream of a NACA 0012 profile and the pressure and density fields are analyzed using digital signal processing methods and digital interferogram evaluation techniques. One of the current results is that a separation bubble is formed at the leading edge of the wing when the vortex passes over the profile. The complicated flow at the boundary of the profile seems to be one of the keys to the understanding of vortex profile interaction.

DD FORM 1473 EDITION OF 1 NOV 65 IS OBSOLETE

UNCLASSIFIED
SECURITY CLASSIFICATION OF THIS PAGE (When Data Entered)

## Summary

The genaral aim of this work is to get more knowledge about aeroacoustic sound generation. To study the strong sound generation in the case of helicopter rotor vortex interaction, a vortex profile flow interaction experiment is performed in a transonic duct. Vortices are generated upstream of a NACA 0012 profile and the pressure field is recorded by a number of transducers. The pressure signals are stored digitally and are processed by a fast digital signal processing hardware to get spectra and correlations. The density fields are recorded interferometrically. An automatic interferogram analysis technique is adapted to the problem to evaluate densities, pressures and vortex traces from the interferograms. One of the current results is that a separation bubble is formed at the leading edge of the wing when the vortex passes over the profile. The complicated flow at the boundary of the profile seems to be one of the keys to the understanding of vortex profile interaction.


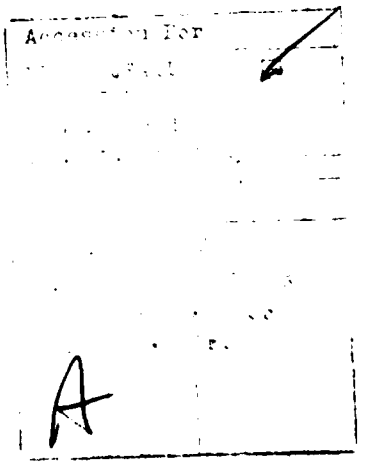

Table of Contents

## 1. Introduction

The aim of this project is to investigate profile flow vortex interaction. Vortex interaction with solid walls generates sound. Vortex noise occurs nearly everywhere in aerodynamics and especially it is one of the helicopter noise sources.

The investigation consists of theoretical calculations and experiments. Especially the unsteady boundary layer behaviour of the profile cannot be predicted, thus experiments must be carried out. Experiments are performed in the transonic duct of the Max-Planck-Institut. Vortices are generated upstream of a profile. Pressure and density fields of the vortex profile interaction are recorded with pressure transducers and interferograms. The interferogram evaluation and the reading of vortex traces from interferograms is supported by a digital technique, developed last years in our department. The automatic fringe evaluation programs have been adopted to the profile flow interferograms and are still under development.

## 2. Experimental Facility

### 2.1. Duct, Vortex Generators and Profiles

The transsonic duct Fig. 1 is a vacuum type wind tunnel with two vacuum tanks of 132 $m^3$ and 24 $m^3$ volume. The maximum measuring time for the profile investigation arrangement is 10 s at Mach 1 and 25 s at Mach 0.3. A new experiment can be performed every 4 minutes (This is the time, the pump needs to evacuate the tanks). For boundary layer control purposes one of the tanks can be used for suction; for blowing there is an pressurized-air supply.

The air is sucked in from the labaratory or an air drying unit. The velocity in the measuring chamber is controlled by an adjustable diffusor. In the smallest cross section of the diffusor the air reaches Mach 1; so there is constant speed throughout the measuring time. The velocity of the air can be chosen from v=0 to v=600 m/s if a Laval nozzle is used [1].

The test section of the duct Fig. 2a,b is 800 mm long, 330 mm high and 100 mm wide. The upper and the lower side of the chamber have slots to provide good acoustical damping. The vortex generators are installed in the 200 mm front section. The profile can be mounted between two windows behind the generators. The windows have a diameter of 230 mm and have interferometric quality. Instead of the windows a pressure measuring plate with an array of holes at 15 mm distance can be used. Up to 16 Kulite transducers are available at present. Thus pressure field recordings can be made.

Two different profiles are used for the investigations. They were made on a numerically controlled shaping machine. They

have a NACA 0012 shape and a cord length of 120 mm and 60 mm length. For investigation they are placed between the windows at different angles of attack.

Two different kinds of vortex generators are used: Bluff bodies, that generate a Karman vortex street, and a profile generating a starting vortex. The upper side of the profile is a flexible membrane. By air pressure the flat membrane bulges. As a bursting membrane is used for pressure supply the bulging process is very fast. At the moment a second model of this type is under investigation (the first one showed flow separation). The profile has a NACA 0018 under side and a flat upper side. It has a nearly symmetrical shape when bulged.

To generate a Karman vortex street for the 120 mm profile a 40 mm cylinder was used. Several shapes of bluff bodies were investigated additionaly to be used with the 60 mm profile. Specially shaped bluff bodies as are used in vortex flow meters and square, triangular, rectangular and circular cylinders of different sizes were tested Fig. 3 . The vortex generators can be placed between the windows for interferometric study or at different positions relative to the profile.

## 2.2. Computer Installation

The experiment computer is a PDP 11/34 with an array processor AP 1208. It has connections to the image processing computer, also a PDP 11/34, to the institute computer, a VAX 11/750, and to the central computer of Göttingen University and Max Planck Institute, a UNIVAC 1100/83. Figure 4 shows the configuration of the PDP and the periphery [2] .

On the right there are the data aquisition components. A CAMAC crate controller (CA11-FP, Digital Equipment) is the interface to 16 transient recorders (Le Croy), a real time clock and a digital I/O port. The transient recorders have 8 K storage capacity of 10 bit data at data aquisition rates up to 1 MHz. They are used to record the pressure data.

An IEC-bus interface is used to record the static pressure with the help of a digital voltmeter.

The third I/O component is the controller (LPA11-K, Digital Equipment) of a 12 bit analog to digital converter. Data rates up to 50 kHz can be stored directly on the disc.

The storage of measured data is performed with a 160 Megabyte disc (System Industries). Long term storage is done with a magtape.

Fast data processing is done with the array processor (Floating Point Systems). It is well suited for fast Fourier transforms, a FFT of 1024 points is done in 3 ms.

For visualization of data there are graphic terminals (VT100 and Tektronix) and a hard copy unit, connected to the computer by a terminal multiplexer.

The interface to the fast data line to the image processing computer is a a DRU-11C (Digital Equipment). A DMC-11 is the interface to the data line to the VAX and UNIVAC. The VAX is

used for program development and other computing purposes. The UNIVAC is needed for DISSPLA plots.

## 2.3. Optical Facility

A Zeiss Mach-Zehnder interferometer can be used for optical investigations Fig. 5 . The channel width is 100 mm. Vacuum in the measuring chamber corresponds to 48 whole fringes in interferograms. The light source is a Fruengel flash bulb. High speed recordings can be made with a rotating drum camera at 10 kHz or with a Fastax camera at speeds up to 8 kHz. Periodic processes are often investigated by single pictures triggered by the computer at a certain phase. This has the advantage of pictures of higher resolution. Figure 6 shows two examples: A NACA 0012 profile at an angle of attack of 10 degrees at a pressure ratio of 0.923, corresponding to a velocity of 110 m/s. The other interferogram is an example of a profile in the turbulent wake of a cylinder at 100 m/s.

## 2.4. Computer-based interferogram evaluation

### 2.4.1. Digitizing and preprocessing

The interferograms are photographically recorded on film by taking single frames or taking series of interferograms on 16mm film using high speed pickup-techniques as described pre-

viously. The digitizing of these interferograms is done by a TV-digitizer, connected to a mini-computer. The resolution is selectable by choice of the scan frequency and the line spacing. Usually a resolution of 512 by 256 points (256 intensity levels) is used, but also 512 by 512 points or even 1024 by 512 points could be achieved. The system further is equipped with a digitizing tablet and a graphic terminal to enable hand input of graphic data. Also, a computer-controlled film projector is used to digitize consecutive frames of a series of interferograms. A detailed description of the system is given in [3,4]. The digitized TV-lines are fed to the computer and are processed sequentially or stored on disk for subsequent processing. Depending on the quality of the interferograms different enhancement procedures can be used to increase the signal-to-noise ratio, to correct an uneven illumination or to increase the contrast of the fringes.

### 2.4.2. Fringe segmentation

The fringe segmentation is performed in two steps. First the gray level fringes are converted to binary levels by using a fixed or floating threshold. In the next step the left- and right-edge points of the fringes are collected and stored in a polygonal data structure using a sequential tracking algorithm. To reduce the amount of data to store, a redundancy reduction process approximates the actual polygon by a subset of the vertices of the original polygon within a given range of tolerance.

If fringes leave the field of view, or if a background object

resides inside the fringe field (e.g., an airfoil), the visible area of the fringes can be handled by using the points on the boundary as edge points of the fringes. The corresponding polygons of course may not be along the boundary of the background object, since they may have different fringe orders. In order to establish the boundary test in a quick, easy and robust manner, it is not desirable to derive the boundary information from the fringe field itself. Instead, the geometry of the test section is used to generate a binary-valued mask, which is compared pixel by pixel with the actual interferogram, while performing the fringe extraction process.

At some locations in the fringe fields the fringe spacing may be very small, as is the case for instance inside the boundary layer, inside a shock wave or near separation lines. If the resolution of the digital system is exceeded at these locations, disconnected or falsely connected fringes may occur. This results in the fact that some of the polygon segments, representing different fringe orders, may be linked together. In order to improve the numbering process, most of the disconnections could be removed by an analysis of some geometrical parameters of the polygons. These geometrical parameters are the shape feature (the circularity defined by the enclosed area divided by the perimeter squared), the ratio of the distance of the polygon endpoints to the length of the polygon line, and the angles between the polygon segments.

Those lines which are suspected to have disconnections are cut by this process at locations where the polygon is folded or where it has sharp edges. The remaining polygons having disconnections not detected by this cutting process have to be handled by the numbering process.

Some consideration and programming work has been done on the problem of getting numbers for the fringe lines of an interference fringe field by using the known numbers of a similar fringe field. The matter is somewhat more complicated, as some of the lines of the actual fringe field may have disconnetions, and therefore it may be impossible to get a unique fringe number for that line.

The idea of a numbering scheme applicable to series of interferograms is to get additional information from the previously numbered fringe field. This may only be possible if the fringe locations vary only a small fraction of the fringe spacing at almost any locations of the test section. If the interframe time between consecutive interferograms is choosen appropriately, this condition is satisfied in the case of the profile flow investigation. The numbering of a series of interferograms starts with the setting of the numbers of the first fringe field by hand. The fringe lines are superimposed by a set of so called test-lines at which a set of order number functions is defined by a rational spline approximation. This set of spline functions is fitted to the fringe lines of the next following interferogram. The numbers of those fringes overlapping uniquely at the test-lines are accepted directly, the other numbers are derived from the spline functions. An older version of the program uses a set of straight lines running in the x- and y-direction, while a newer version, currently under development, uses a set of polygons as test-lines. The advantage of the polygonal test-lines is that they are more suitably adaptable to the global course of the fringe lines.

In the case where some disconnected lines remained from the preprocessing step these lines may not receive a unique number

by the numbering scheme. To decide where these lines have to be divided into two or more segments - an older version of the program uses the angles between subsequent polygon segments - the deviations from a local approximation of the fringe order function is used. Another advantage of comparing fringe fields by using local polynomial approximations is the fact that fringe polygons, having no intersections with the test-lines, could be processed with the same algorithm, leading to a more stable behaviour of this numbering process.

### 2.4.3. Polynomial approximation

The fringe order function is defined at a set of contour lines, but most of the mathematical transformations to follow require the interpolation of fractional fringe order numbers. Some methods to interpolate between randomly scattered points on a surface are discussed in the literature [5]. We have used a local distance weighted polynomial least squares approximation, best suited in regard to computation time and numerical representation. This process computes the coefficients of two-dimensional polynomials of second order at the meshpoints of a rectangular grid. To calculate the interference order inside the meshes, the four polynomials at adjacent corners of the mesh are evaluated and weighted proportional to their distance to the point of interest.

Another method is to compute a two-dimensional spline approximation, using some of the previously computed polynomial coefficients, to get a smooth surface having continuous first and second derivatives. The density function may easily be com-

puted by a linear transformation of the fringe order values, because in the actual experimental set-up the fringes are lines of constant density (infinite fringe case). In the case of finite fringe fields a subtraction of the overlayed fringe pattern could be achieved by a modification of some of the polynomial coefficients.

### 2.4.4. Localization of the vortex core

In the current study of the vortex profile interaction process a point of interest is the knowledge of the vortex traces under different positions of the profile, to see if a theoretical description of these traces is in accordance with experimantal results. Some program development has been done to localize the typical fringe pattern resulting from the appearance of the vortex. The vortex core is computed using the centroid of the enclosed area of the innermost of these fringe lines.

# 3. Testing of Vortex Generators

## 3.1. Single Vortex Generator

The first model of the membrane starting vortex generator did not generate vortices. Interferograms showed a turbulent wake, which was caused by a too high angle at the trailing edge. But the componennts of the apparatus had a good technical performance. A movie, taken at 8000 frames per second with the fastax camera, showed the fast rise time of 0.5 ms and a decay of mechanical oscillations of the same order of magnitude. Before building a second vortex generator, a model of the new profile shape was tested in the transonic duct. There was no separation at any speed. This vortex generator is still under test, but it does not yet work satisfactorily.

## 3.2. Vortex Street Generators

Vortex streets should be two-dimensional, should have a constant Strouhal number and must consist of strong potential vortices of the right spacing to be of use in our experiment. The interaction of vortices among themselves should be less than the interaction of profile and vortex. This means, that the quotient length/(2*Strouhal number), the spacing of the vortices, should be at least of the same magnitude as the profile length. The 40 mm cylinder has a Strouhalnumber of 0.2 and shows a vortex spacing of 40/(2*0.2)=100 mm Although the aspect ratio of this cylinder is very small, the vortex street is quite stable and has only a single main frequency.

Figure 9a shows the frequency at different pressure ratios. The Strouhal number is nearly constant but there is some influence of resonance of the duct geometry.

As interferograms show Fig. 7a,b strong vortices are produced immediatly downstream of the cylinders. Unfortunately there is a rapid diffusion of vortex strength and the shape of the vortex street does not remain constant. But there is an intermediate region behind the cylinders, where the vortex street is two-dimensional and the vortices still have a small core Fig. 7c .

The 40 mm cylinder and the 120 mm profile were taken for the first profile vortex interaction tests. The distance between the cylinder axis and and the profile nose has been 210 mm. Figure 9b shows the arrangement is working with an even higher amplitude than the pure cylinder.

For tests with the 60 mm profile several bluff body shapes were investigated Fig. 3 . The 20 mm circular cylinder does not work as good as the bigger one, maybe because of a different aspect ratio. It turned out that a square cylinder at right angle of the front surface plane to the flow has the highest amplitudes and best constancy of Strouhal frequencies over the Reynolds number range.

# 4. Experimental and Theoretical Results

## 4.1. Vortex Traces

To evaluate vortex traces and sound generation a simple model of profile vortex interaction is used. It consists of potential theory and is evaluated by conformal mapping. Compressibility, boundary layer effects and the Kutta condition are not included. This is of course a very crude model and we do not assume that the mentioned effects are of no importance in the problem. But there is no experience what the Kutta condition is like in the instationary case. There are also no predictions about boundary layer effects such as separation or secondary vortex generation, which perhaps might happen. Because we do not know much about what really happens, we started with a rather simple model, which shall be of some use in comparisions with the experiment, although it can not be an exact description of the problem. The model has the advantage that computation is not too difficult and that an evaluation of sound generation is possible by matched asymptotic expansions.

A vortex and its mirror image are transformed by conformal mapping to a vortex near a cylinder. After adding a flow velocity v and changing the position and radius of the cylinder a Joukowsky transformation is applied. The result is a vortex in the vicinity of a Joukowsky profile. The properties of the profile depend on the position and radius of the cylinder. The angle of attack is choosen to be zero. The thickness parameter L and the trailing edge roundness parameter R are arbitrary. L=1 and R=0 give a flat plate; L=1.075 and R=0.038 give a NACA 0012 like shape.

The motion of the vortex is evaluated with the help of a Hamilton function with a Runge-Kutta algorithm. The whole hydrodynamic field can be evaluated. An example of evaluated vortex traces is given in Figure 8. The dimensions of the profile and the circulation of the vortex are similar as in the interferograms. Several vortex traces with different starting points are plotted as dashed lines. The solid lines are streamlines of the undisturbed flow. The experimental conditions are represented by the vortex trace directly under the profile. The traces above the profile correspond to other relative positions of profile and vortex generator.

The time dependent hydrodynamic far field can be matched to the sound field by matched asymptotic expansions. The result of the first order is a dipol-like field [6,7,8,9,10].

## 4.2. Pressure Measurements of Vortex Profile Interaction

Measurements were performed with the 40 mm cylinder with and without the 120 mm profile. The pressure ratio range was from 0.999 to 0.6, that is from 13 m/s to 290 m/s.

As expected, the pressure field is antisymmetric, when vortex generator and profile are aligned in the cordplane. The difference from antisymmetry is less than 5 degrees phase angle in Fourier spectra. Therefore it is sufficient to have pressure transducers only in the upper half of the measuring chamber.

Figure 2b shows the pressure transducer positions used in the measurements which are described in this report. Figure 9 is recorded with pressure transducer 5. Figure 10a and b are typical examples of pressure recordings. At a pressure ratio of 0.83 transducer 2 measures an underpressure of more than 200 mbar. The vortices differ in strength and do not have the same path, so the extreme underpressure peaks only happen from time to time. There is a diffusion of vortex strength and the signals at transducers 8,10 and 12 do not have such high amplitudes anymore. Signals at transducers 5,6,7 and 9 (above profile) do not have single peaks anymore but a more sinusoidal shape.

Depending on duct resonance effects the peaks of frequency recordings are more or less sharp. But there is always a Strouhal frequency signal far above the wall turbulence level at nearly all measuring points. Figures 11 to 14 are typical examples of spectra. The spectra are done with 0.8 s long pressure recordings at 10 kHz sample frequency.

At the same pressure ratios vortex street and profile vortex interaction have the same Strouhal frequency. The vortex generation process seems to be not influenced by the profile. The profile measurements show only a slightly better constancy of Strouhal frequency. The amplitudes in the vicinity of the cylinder are of the same order of magnitude. The amplitudes measured above the profile (transducers 3,5,6,7,9) are much greater in the profile case. At any pressure ratio the phase differences between the measuring points are entirely different. The hydrodynamic field as well as the sound field are influenced strongly by the profile.

The first pair of spectra Fig. 11 is done at the high pressure ratio of 0.998. The velocity is about 19 m/s. The sound generation is inefficient at low velocities. The pressure field is a relatively undisturbed hydrodynamic field. The Strouhal frequency is of the same magnitude in both cases, but the vortex street signals are more noisy. Very obvious is the difference at transducer 1. Only transducer 8 of the profile case shows a noisy character, because it is influenced by the profile wake. It is interesting that the phase differences between the same transducer pairs are entirely different even in the pure hydrodynamic case.

The second pair of spectra Fig. 12 has a sharp dominant frequency with the profile and several frequencies with the vortex street, due to beats and frequency jumps. Figure 13 is an opposite example. The vortex street shows the more narrow frequency band, whereas the profile has got a large number of different Strouhal frequencies. Surprisingly there is the same dominant frequency at all measuring points.

Figure 14 is a resonance case with extremly high amplitudes. There is the same frequency at all measuring points and nearly the same frequency in both plots (The first harmonic has a higher amplitude at transducer 1 and 8, but the fundamental is the same). In both cases highest amplitudes are at transducers 2 and 3. The transducersignals above the profile (3,5,6,7,9) have higher amplitudes with the profile. The greatest difference is in the first harmonic Fig. 15 . There is a harmonic at transducers 1,2,3 in both cases, but the profile shows higher amplitudes and higher quality factor. Entirely different are the transducersignals above the profile (5,6,7,9) where the vortex street shows noise and the profile shows the first harmonic with high amplitudes and high quality

factor. This might be a hint that a new phenomenon is ocurring with strong vortices at high Reynolds numbers.

## 4.3. Pressure Fields

Acoustics are of less importance at low velocities. The pressure field is a nearly hydrodynamic one. This makes the understanding of the pressure field easier and is a first step to the solution of the problem. When the hydrodynamic field is estimated, properties of the acoustic pressure field can be evaluated by subtracting the hydrodynamic field from the measured pressure field.

First investigations of pressure fields at low velocities are made. To get phase differences, Fourier transforms and correlation techniques are used. Vortex streets have a nearly constant pattern, that moves downstream with flow velocity. Equal phase lines are straight lines at a right angle to the velocity direction.

Phase maps of profile-vortex interaction look different. Transducers above the profile (4,5,6,7,9) measure only very little phase differences. The differences are in the range of about 10 degrees. That is nearly the same order of magnitude as the differences from one measurement to another. So until now we do not have exact phase maps of profile case. But we can make the interesting statement that the upper side of the profile is nearly an equal phase region at low velocities. All this is caused by the change from the hydrodynamic pres-

sure fluctuations without profile, which move with flow velocity, to the unsteady mixed hydrodynamic acoustic wave field in case of profile interaction.

Acoustics are of much more influence at higher velocities; phase maps look different and are more complicated. To get exact phase maps the grid of transducers must be very narrow. Further experiments must be made.

## 4.4. Interferograms

Figure 16a, b *and* c *are* interferograms of profile-vortex interaction. Not all the interferograms show single vortices because sometimes the vortex street shape changes to turbulence. Figure 6b is an example for turbulent flow. All the interferograms are taken at a velocity of 100 m/s. The pressure difference between stagnation point pressure and undisturbed flow pressure corresponds to 4 half density fringes. No triggering was applied, so the phase is arbitrary. Pictures of different phases are arranged so that Figure 16 shows the passing of a vortex beneath the profile. Figure 16a shows a vortex in the vicinity of the leading edge. There is a tiny suction peak on the vortex side of the leading edge. The suction peak grows until the vortex reaches the middle of the profile Fig. 16b , but there is no suction peak any more when the vortex has passed this point. Up to this point the vortices seem to be of similar strength. But we do not find any strong vortices in the vicinity of the trailing edge anymore under these experimental conditions. As shown in Figure 16c the vortex obviously generates a separation bubble which

influences the suction peak and possibly the vortex strength.

The interferograms show that the vortices have a strong influence on the profile flow and vice versa. The flow around the leading edge and the stability of the vortex seem to be important properties of the interaction phenomenon [11,12].

## 4.5. Evaluation of interferograms

As an example of the digital interferogram analysis two processed fringe fields of a profile flow with and without a vortex present are shown in Figures 17a and 18a. The flow velocities are 280 m/s respectively 100 m/s at an angle of attack at 0 degrees. The interferograms where digitized with a resolution of 512 by 256 pixels. The fringe extraction process described in chapter 2.4 was used to obtain the polygonal fringe fields shown in Figures 17b and 18b. The boundaries of the test-section as well as the airfoil are input by hand, using the digitizing tablet. These lines are used to prepare a mask file, needed by the fringe extraction program to avoid connections of fringe lines along the boundaries of background objects. Due to the restricted resolution of the digital system there appeared some falsely connected lines around the leading edge of the airfoil, where the fringe spacing is very small. These locations could be detected and the falsely connected lines could be cut by application of the aforementioned algorithm, using the geometrical parameters of the lines.

The lines are numbered corresponding to the interference

order, which in this case is done by hand, because the automatic numbering algorithm, applicable to these types of fringe fields, needs a numbered field to start the numbering process of consecutive frames. The density function was derived from the fringe field by approximation of polynomials of second order at the mesh points of a rectangular grid (shown in Figs. 17b and 18b) as decribed in chapter 2.4. To achieve a smooth surface, the interference order function was calculated from these polynoms by use of a bicubic spline interpolation procedure. Two density profiles in x-direction at y = 0.2 are plotted in Figs. 17c and 18c. The realtive density as a function of the fringe order is given in this case as

$$\varrho/\varrho_0 = 1 - \frac{1}{n_0(T_E,\ p_E) - 1}\ \frac{p_E}{T_E}\ \frac{T_0}{p_0}\ \frac{\lambda}{h}\ \frac{N(x,y)}{2}$$

where $\varrho/\varrho_0$ is the relative density, $n_0(T_E, p_E)$ is the refractive index of air at temperature $T_E$ and pressure $p_E$, $T_0$ and $p_0$ are the temperature and pressure at rest, $\lambda$ is the wavelength of light, h the depth of the test chamber and N(x,y) the fringe order function. Note, that the order function is divided by two, because each fringe is represented by two lines (a "left" and a "right" one). The above equation, evaluated with the actual dimensions valid in the tests, yields

$$\varrho/\varrho_0 = 1 - 0.01058 * N(x,y).$$

As can be seen from Fig. 18, the lowest density appears inside the vortex core with a value of 0.92 relative to the density at the stagnation point, where the fringe order was set equal to zero.

## 5. Conclusions and Plans

The complicated flow at the boundary of the profile seems to be one of the keys to the understanding of vortex profile interaction. Interferograms are well suited for the investigations of these effects. We are confident that further improved experiments with the vortex profile interaction will give us a better insight in the details of near field flow.

Some more work has to be done to evaluate the sound field. New experiments with single vortices will be carried out. Technical requirement is a further development of single vortex generators. Great importance is attached to this subject. New techniques like suction boundary layer control will be tested.

Concerning the digital evaluation of interferograms some further development of automatic fringe numbering and trace following algorithms will be done. For a representation of the fringe order function, respectively the density or pressure function, the polynomial patches will be computed on an irregular net better adapted to the actual flow field, using meshes of smaller size at the region of the leading edge of the airfoil.

## 6. References

[1] Meier, G.E.A.: Ein instationäres Verhalten transsonischer Strömungen. Mitteilungen aus dem MPI für Strömungsforschung und der AVA, 1974, Nr. 59.

[2] Rehberg, I.: Eine strömungsakustische Spitzenkatastrophe. Mitteilungen aus dem MPI für Strömungsforschung und der AVA, 1983, Nr. 75.

[3] Becker, F., Zur automatischen Auswertung von Interferogrammen, Mitt. Max-Planck-Institut für Strömungsforschung Göttingen, Nr. 74, (1982)

[4] Becker, F.; Meier, G.E.A.; Wegner, H., Automatic evaluation of interferograms, Applications of Digital Image Processing IV, Andrew G. Tescher, Editor, Proc. SPIE 359, pp. 386-393 (1982)

[5] Schumaker, L.L., Fitting surfaces to scattered data, In: Lorentz, G.G.; C.K. Chui; L.L. Schumaker, Approximation Theorie II, Academic Press (1976), pp. 203-268

[6] Obermeier, F.: On a New Representation of Aeroacoustic Source Distribution. I General Theory. Acustica 1979/42, pp. 56-61.

[7] Obermeier, F.: On a New Representation of Aeroacoustic Source Distribution. II Two-dimensional flows. Acustica 1979/42, pp. 62-71.

[8] Möhring, W.: On Sound Waves in Shear Flow. Max-Planck-Institut für Strömungsforschung, Bericht 111/1976.

[9] Obermeier, F.: The application of Singular Perturbation Methods to Aerodynamic Sound Generation. Lecture Notes in Mathematics. Vol. 594, Springer Verlag (1977), pp. 400-421

[10] Obermeier, F.: Zur aerodynamischen Schallerzeugung wirbelbehafteter Strömungen in der Umgebung starrer Körper. Max-Planck-Institut für Strömungsforschung, Bericht 106/1978.

[11] Ziada, S. and Rockwell, D.: Vortex-leading-edge interaction. J.Fluid.Mech.(1982),vol. 118, pp. 79-107.

[12] Tang, Y.-P. and Rockwell, D.: Instantaneous pressure fields at a corner associated with vortex impingment. J.Fluid.Mech.(1983), vol. 126, pp. 187-204.

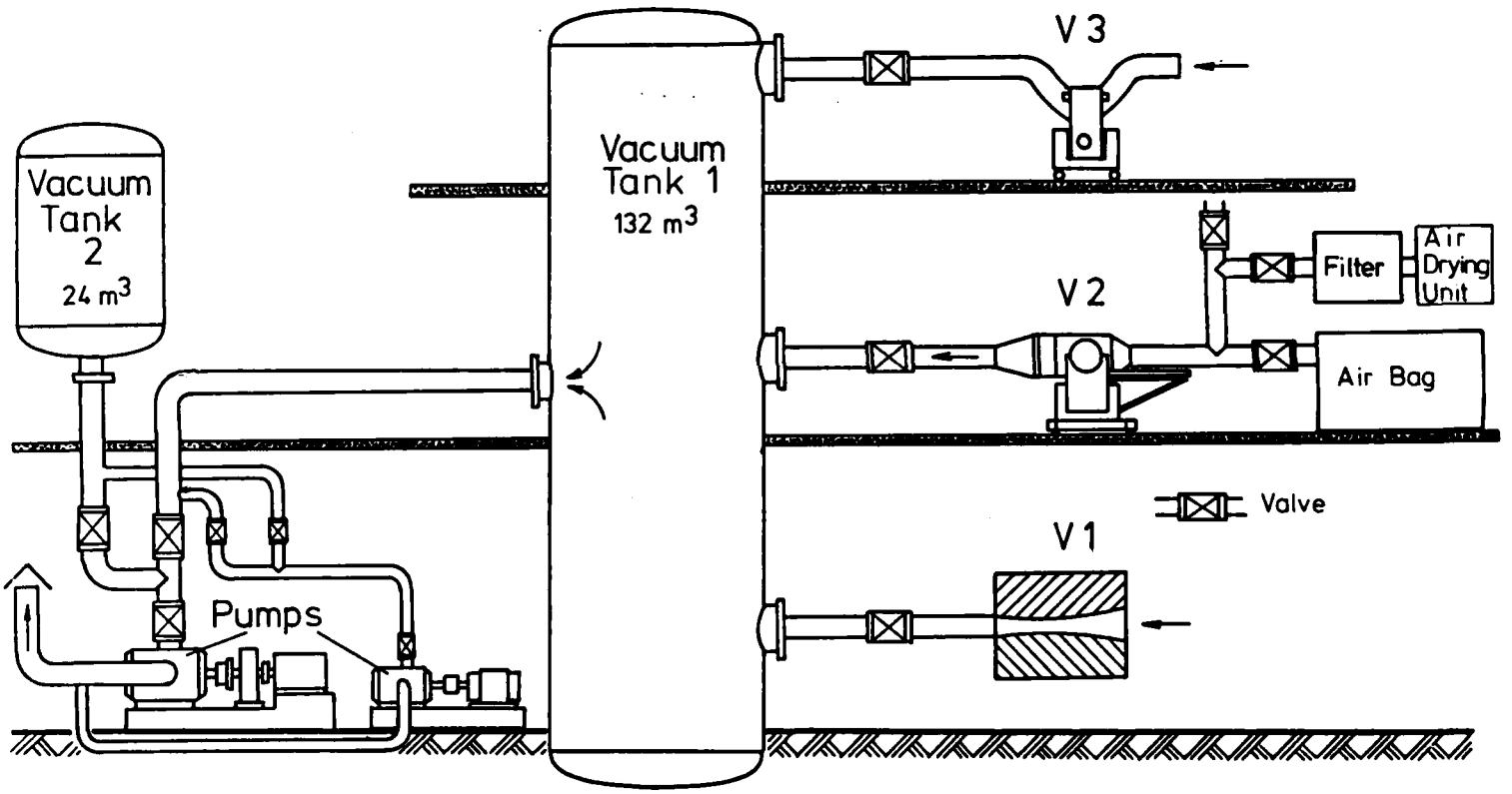


Figure 1: The transonic duct. Experiments are carried out at facility V2.

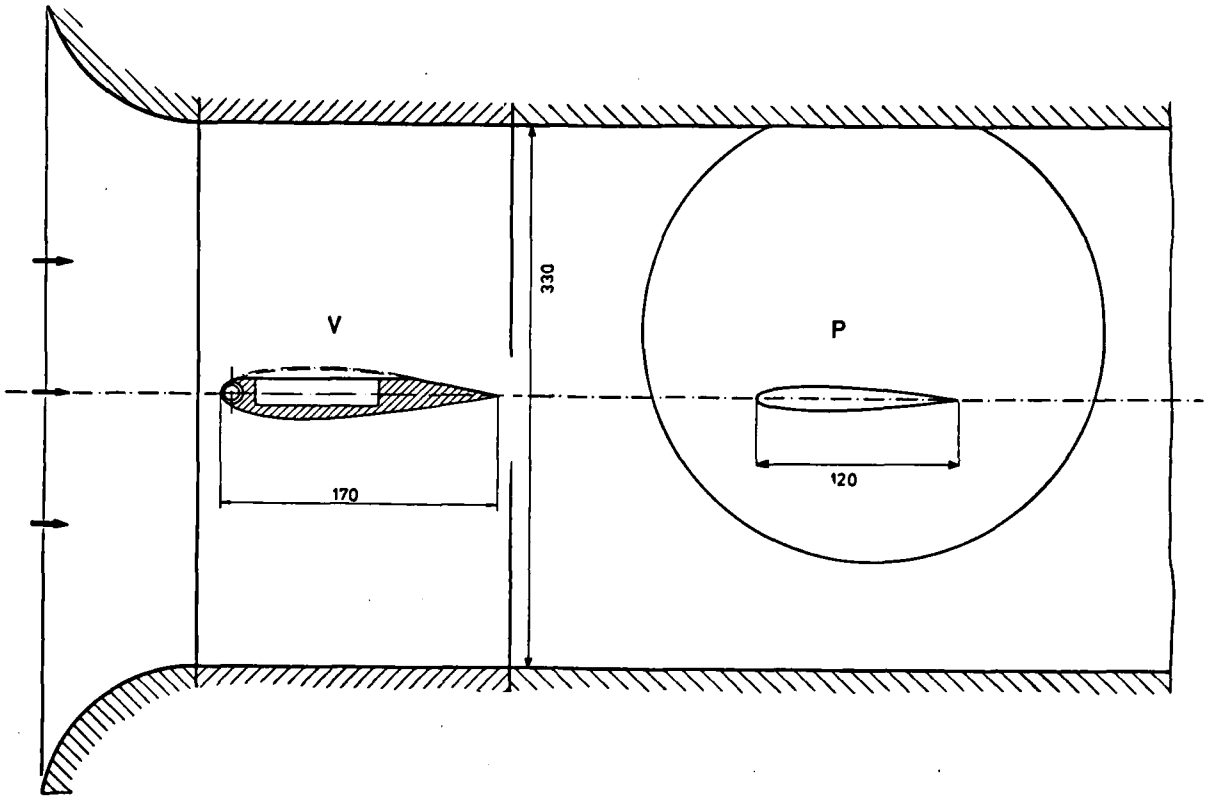


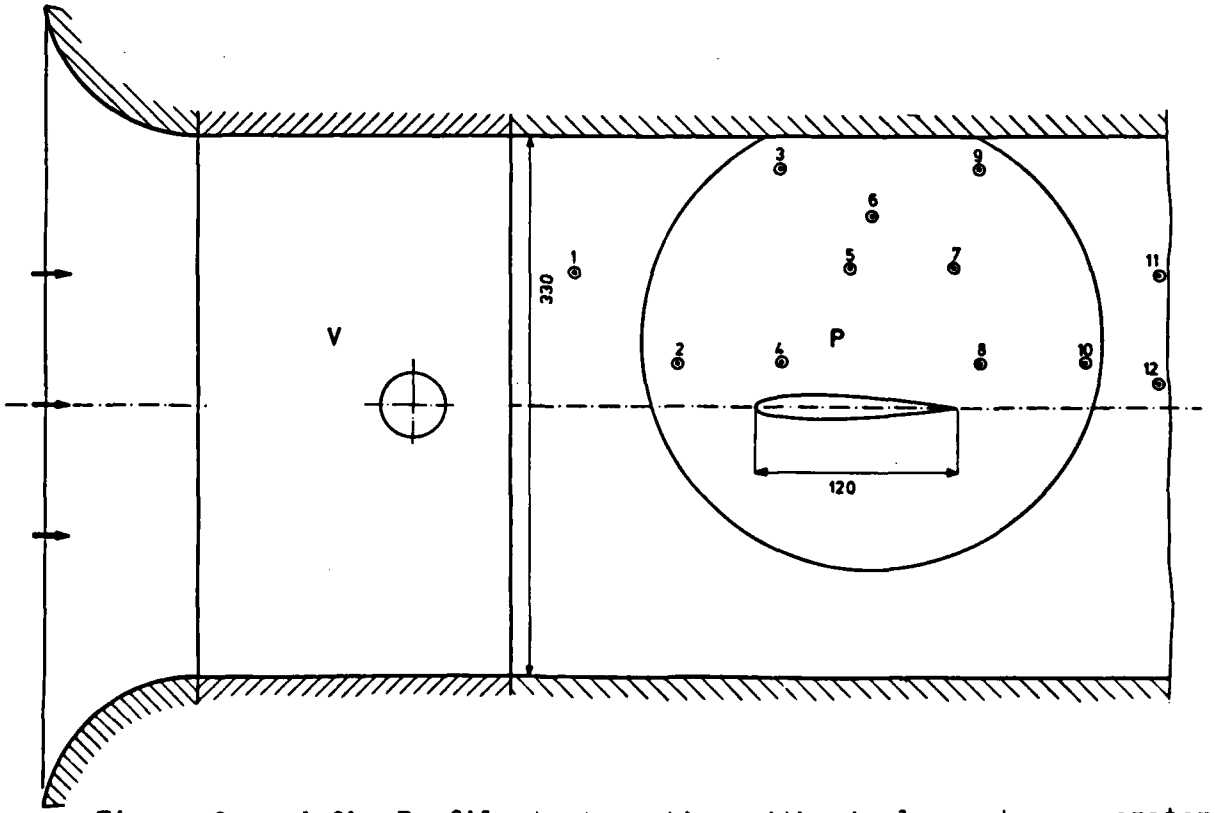


Figure 2a and 2b: Profile test section with single vortex generator (2a) and cylinder (2b). Points 1 - 12 are transducer positions.

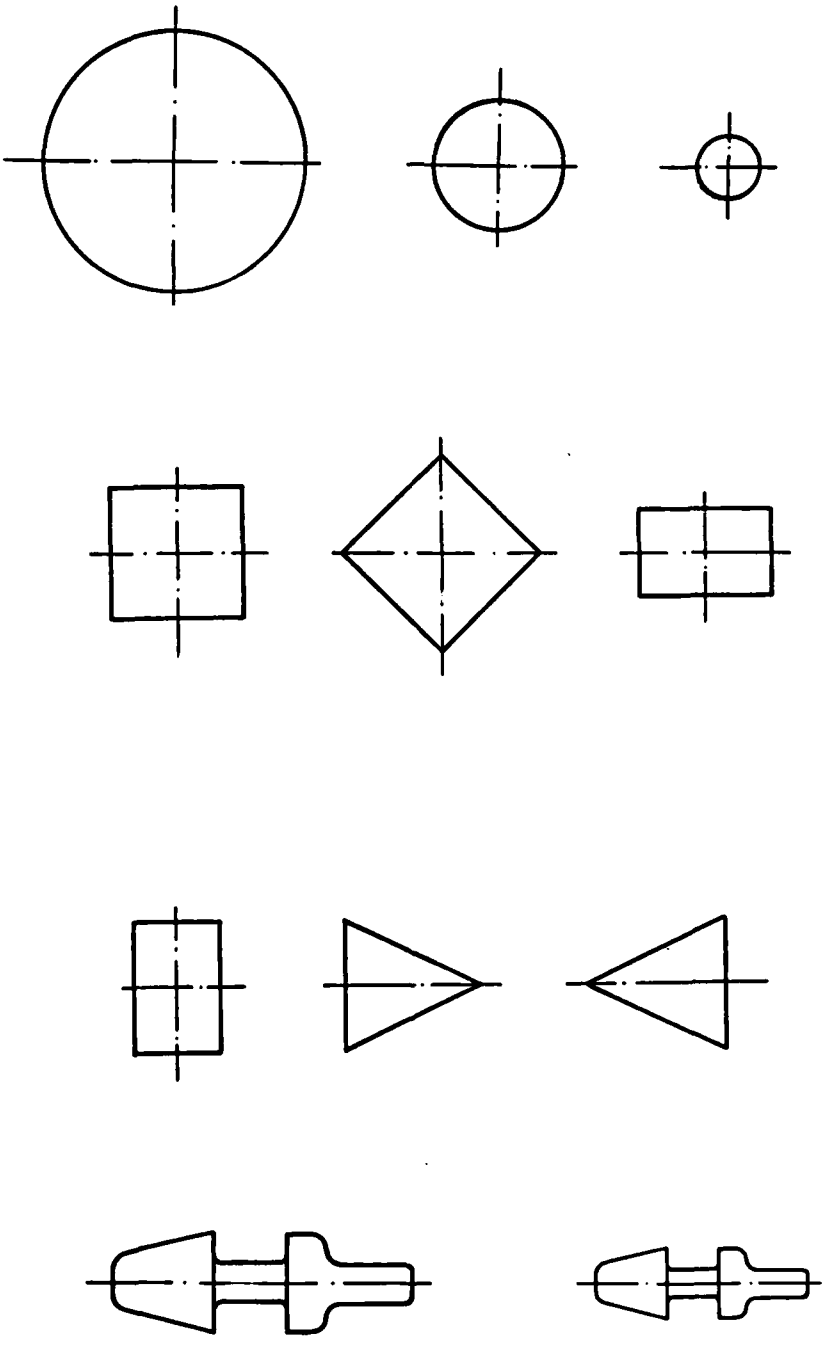

Figure 3: Vortex street generators:
Cylinders of 40, 20 and 10 [mm] diameter,
square and rectangle of 20 [mm] width,
rectangle and triangles of 20 [mm] height
and flow meter vortex generators.

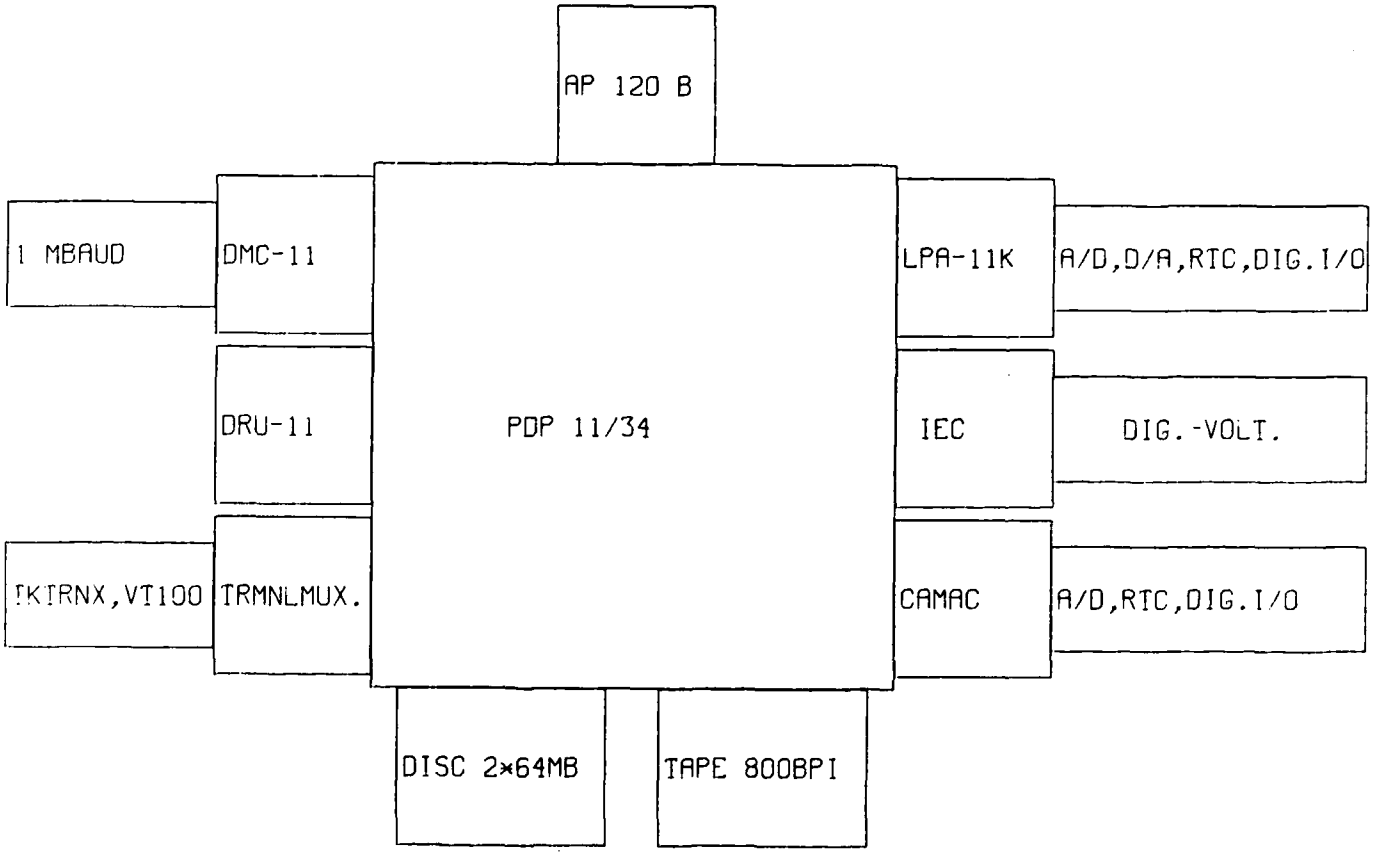


**Figure 4: Computer installation.**

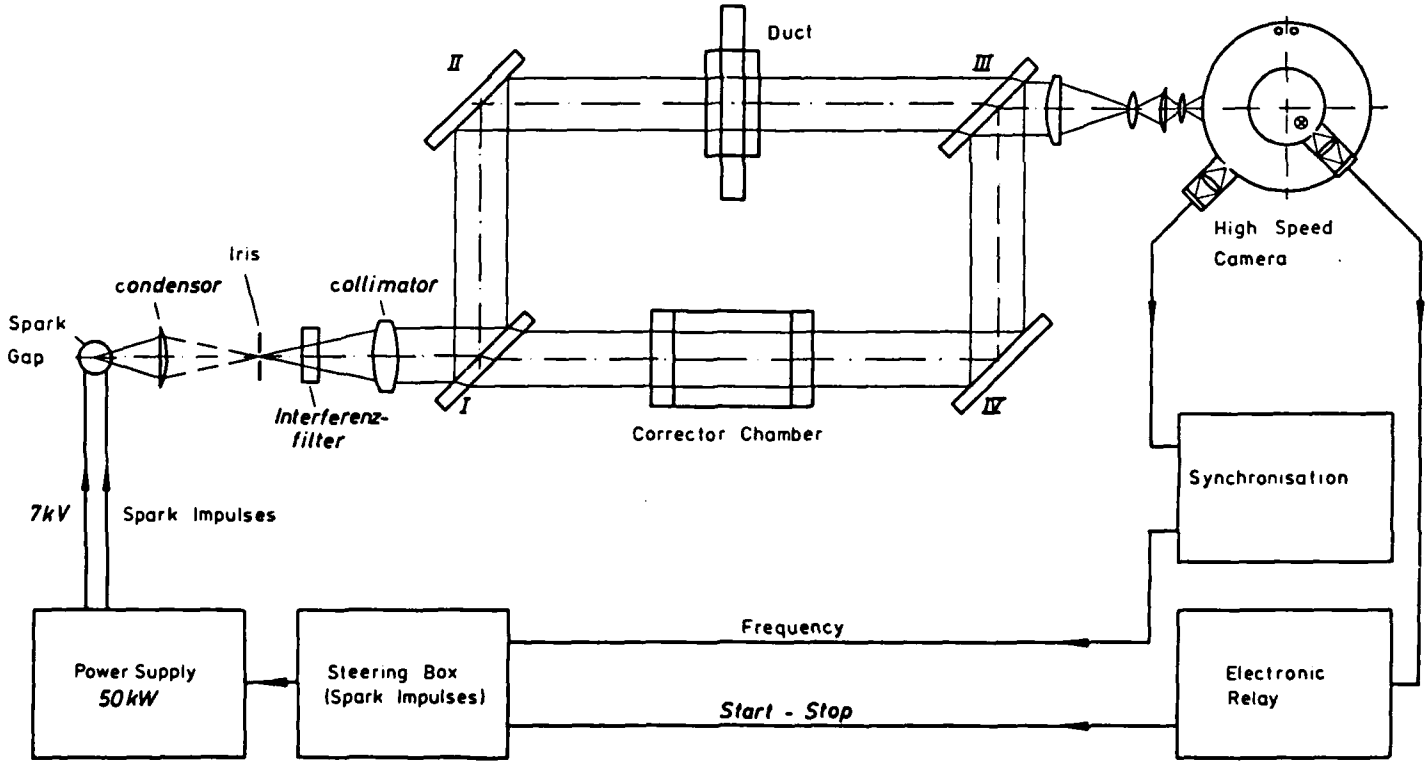


Figure 5: Optical facility for high speed interferogram movies.

Figure 6a and 6b: Interferograms of a NACA 0012 Profile at 10 degrees angle of attack at 110 [m/s] and the same profile in the turbulent wake of a cylinder at 100 [m/s].

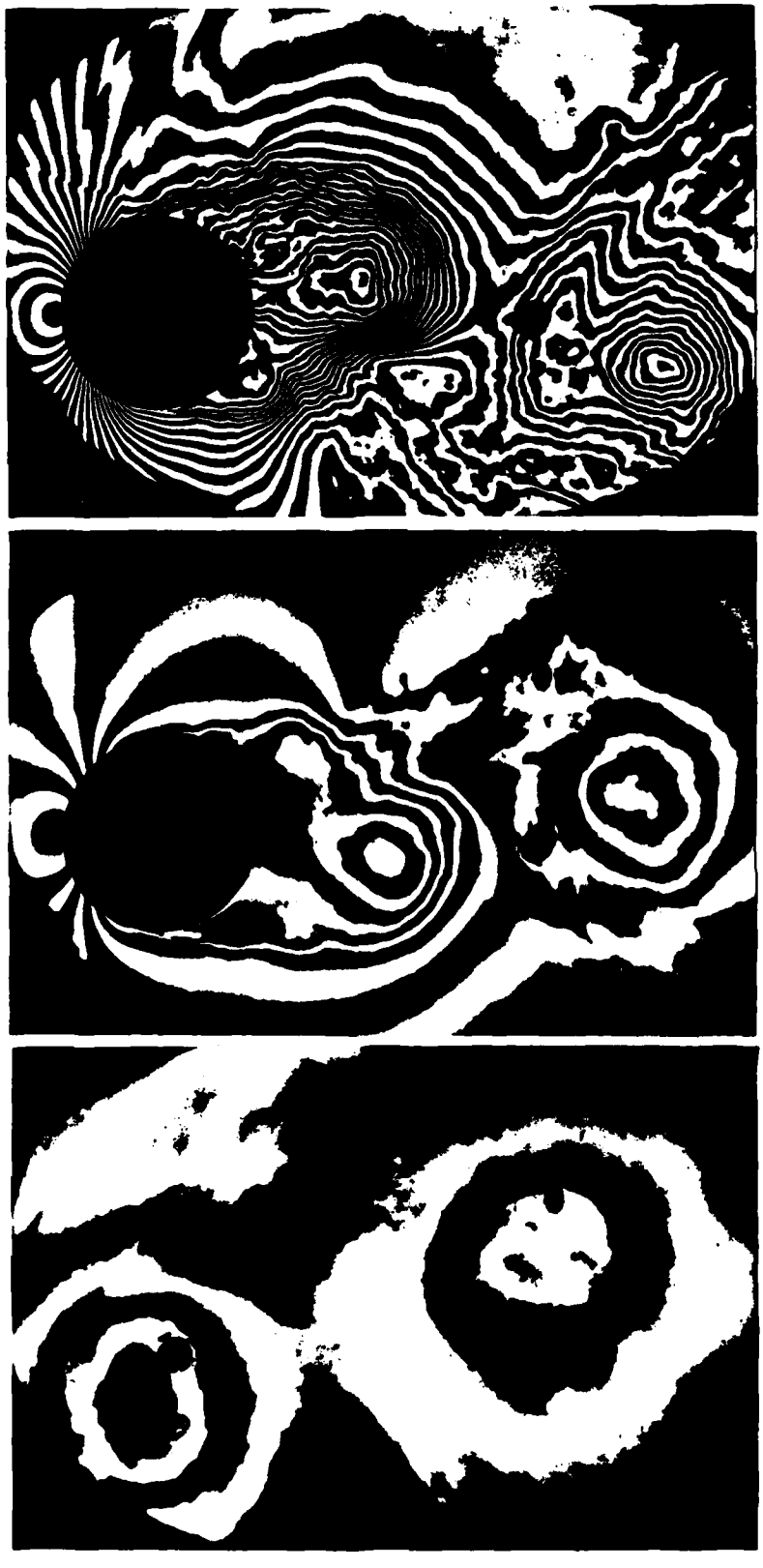

Figure 7a, 7b and 7c: Interferograms of a vortex shedding 40 [mm] diameter cylinder at 200 [m/s] and 100 [m/s]. 7c shows the vortex street at 100 [m/s], the cylinder is mounted 180 [mm] upstream as in Figure 2b. (The dark spots are holes in the window, where the wing can be mounted.)

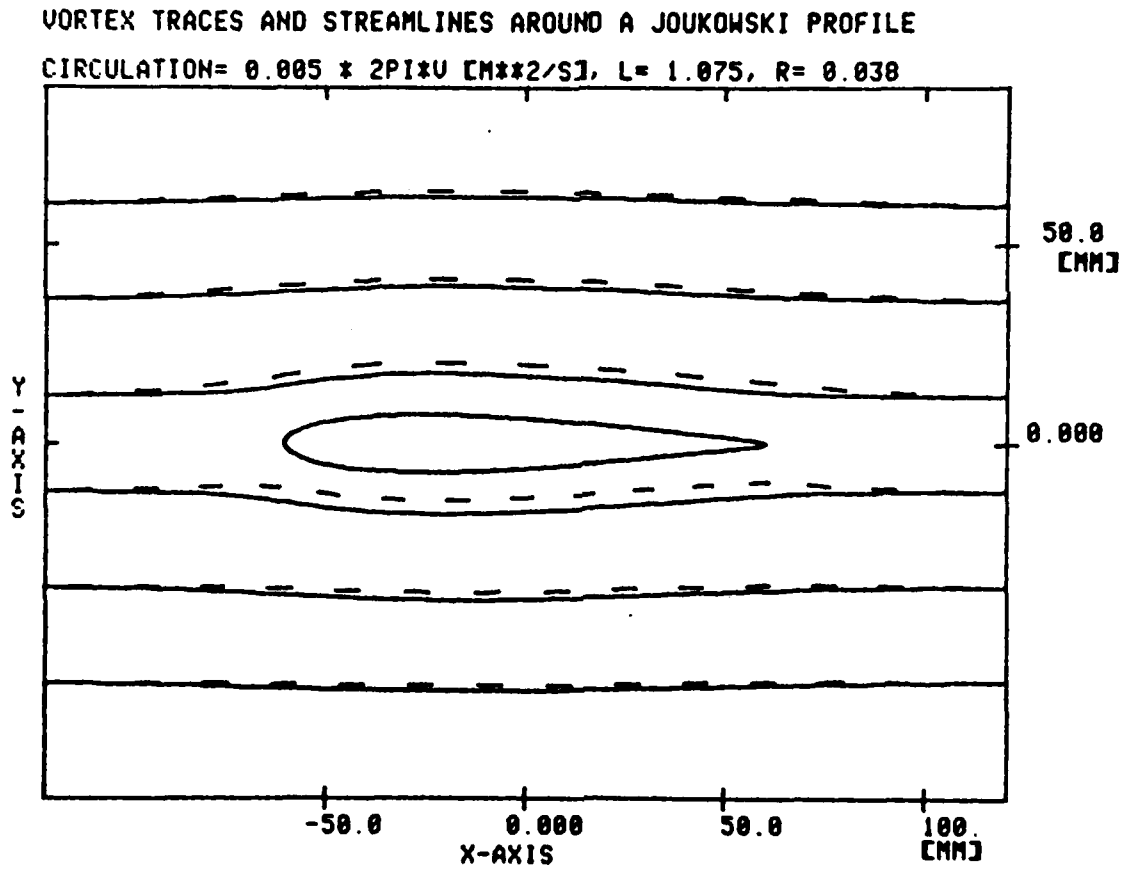


Figure 8: Vortex traces evaluated with potential theory.

Figure 9: Fourier spectra at different pressure ratios.

9a: Vortex street
Transducer 5 Maximal Amplitude: 14.17 [mbar]

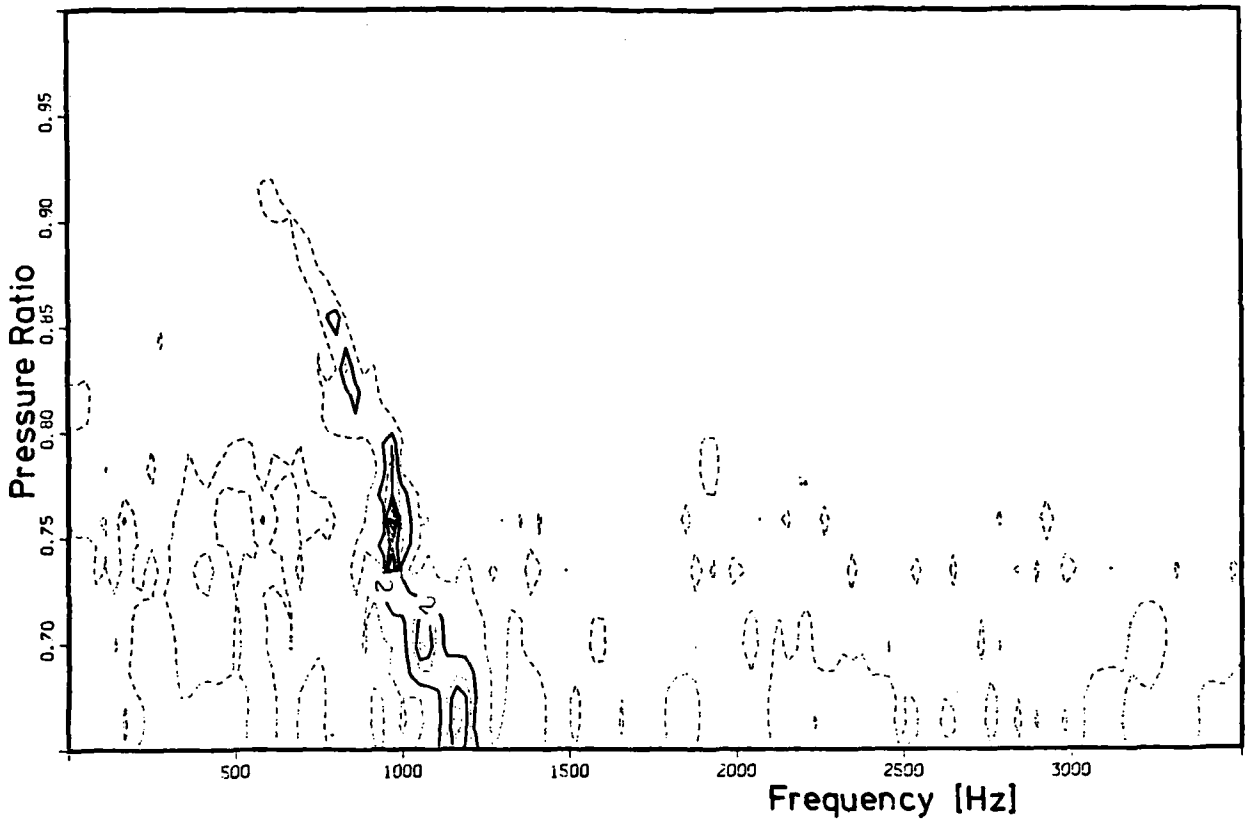


9b: Profile - Vortex Street Interaction
Transducer 5 Maximal Amplitude: 49.92 [mbar]

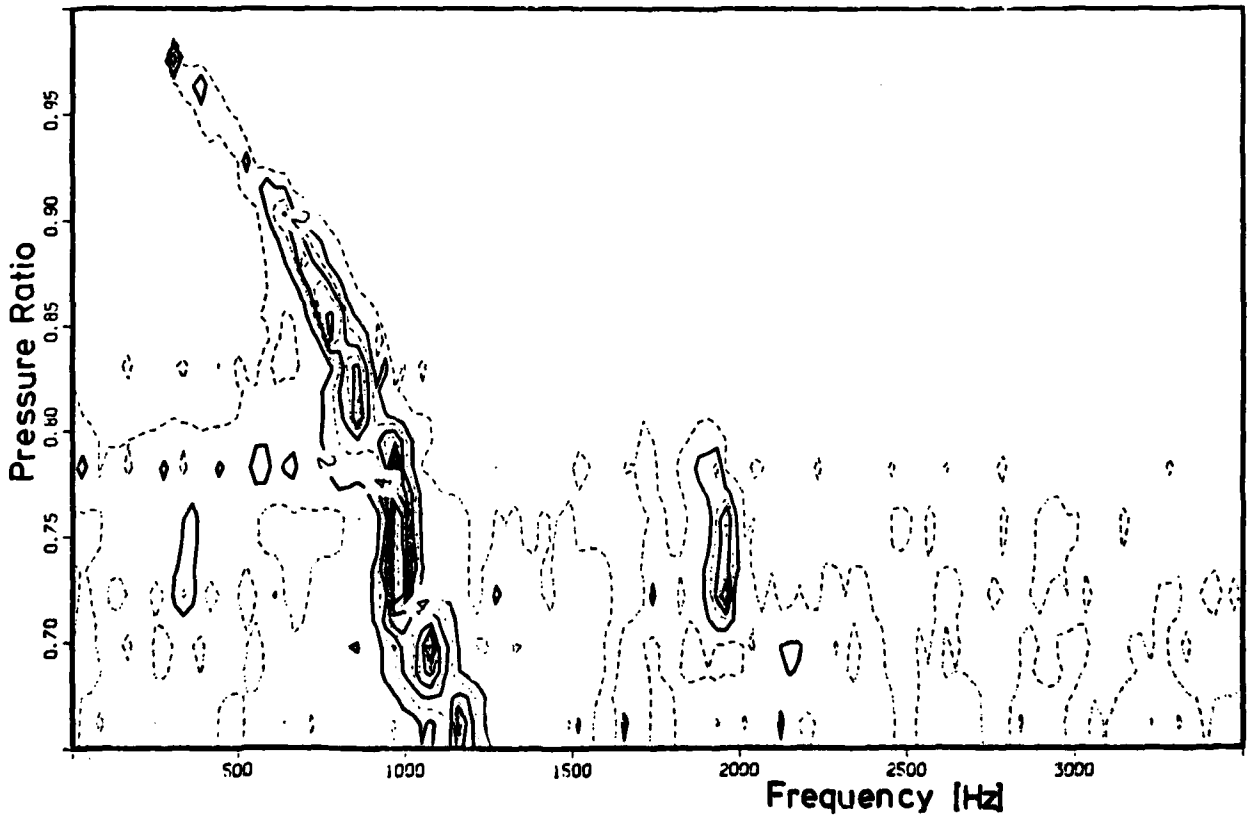

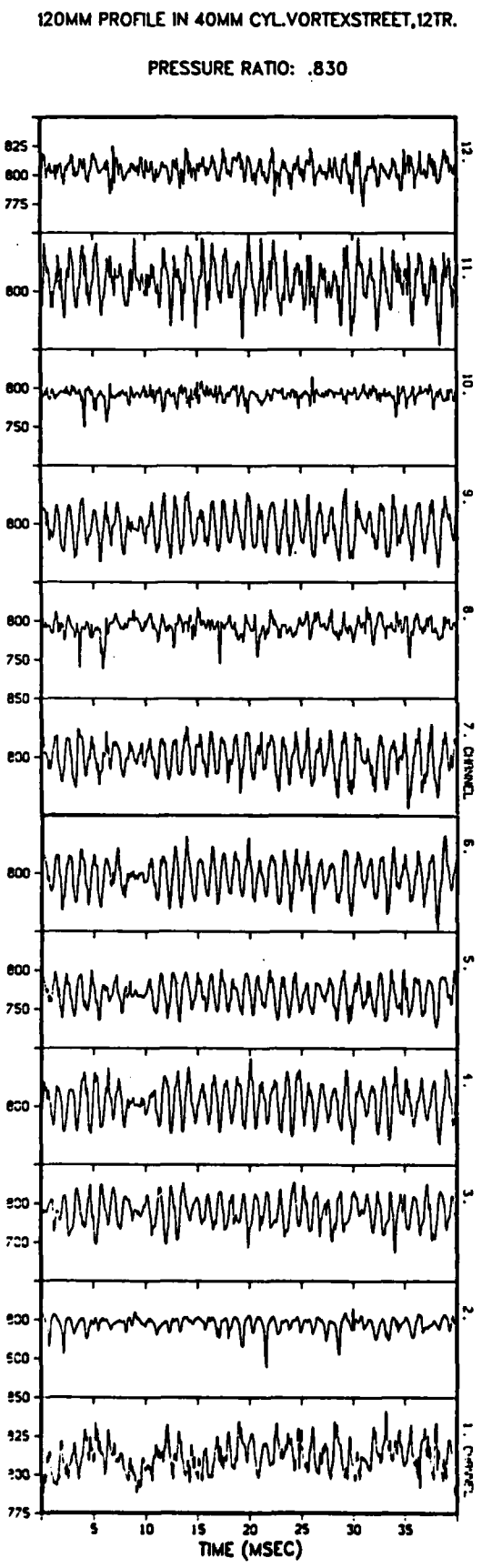


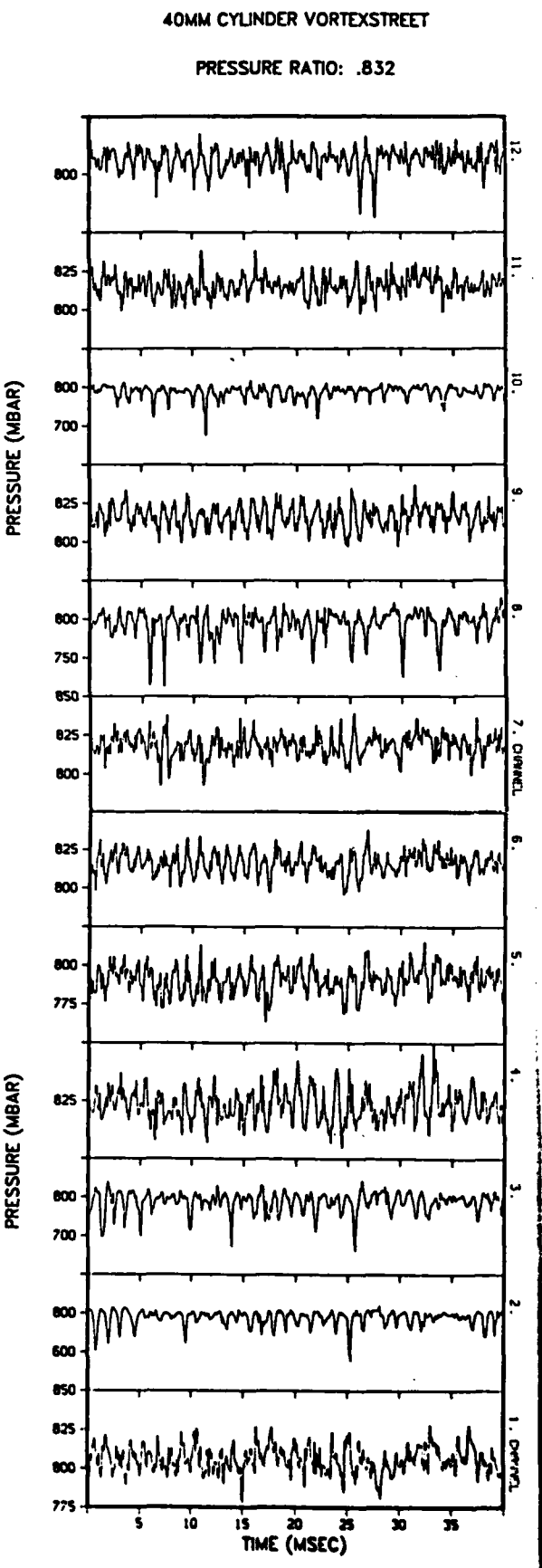


Figure 10a and 10b

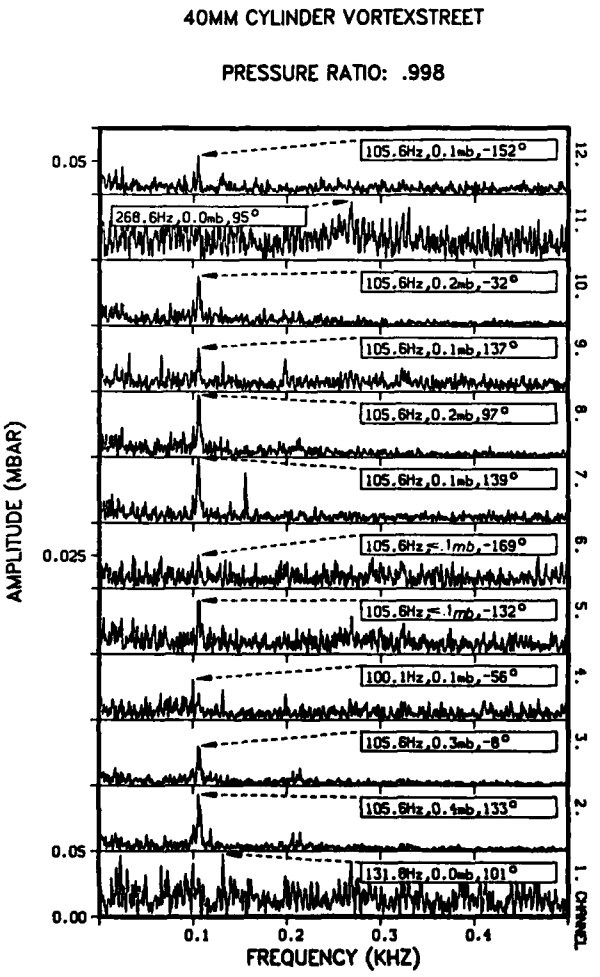


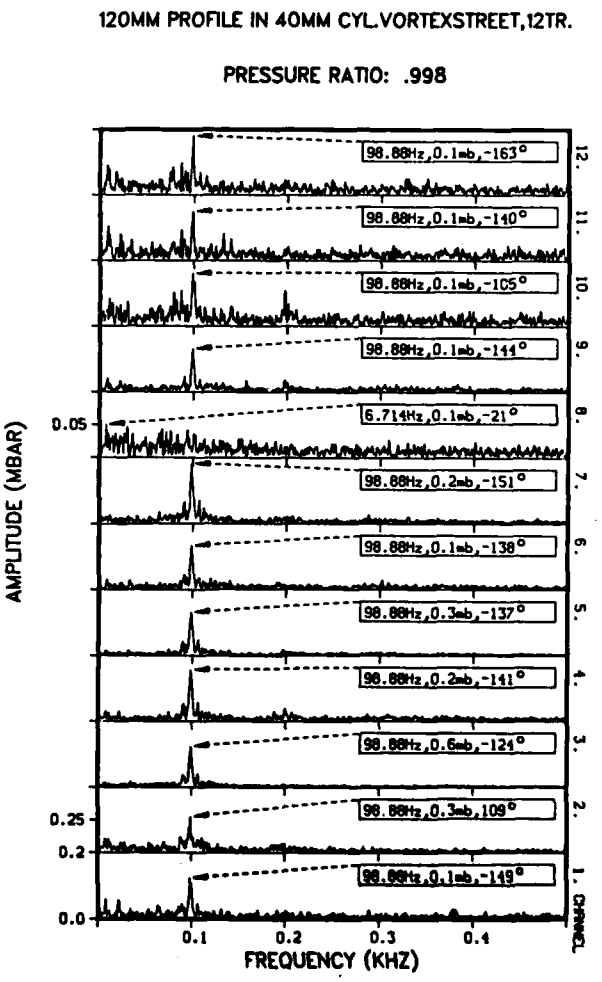


Figure 11a and 11b

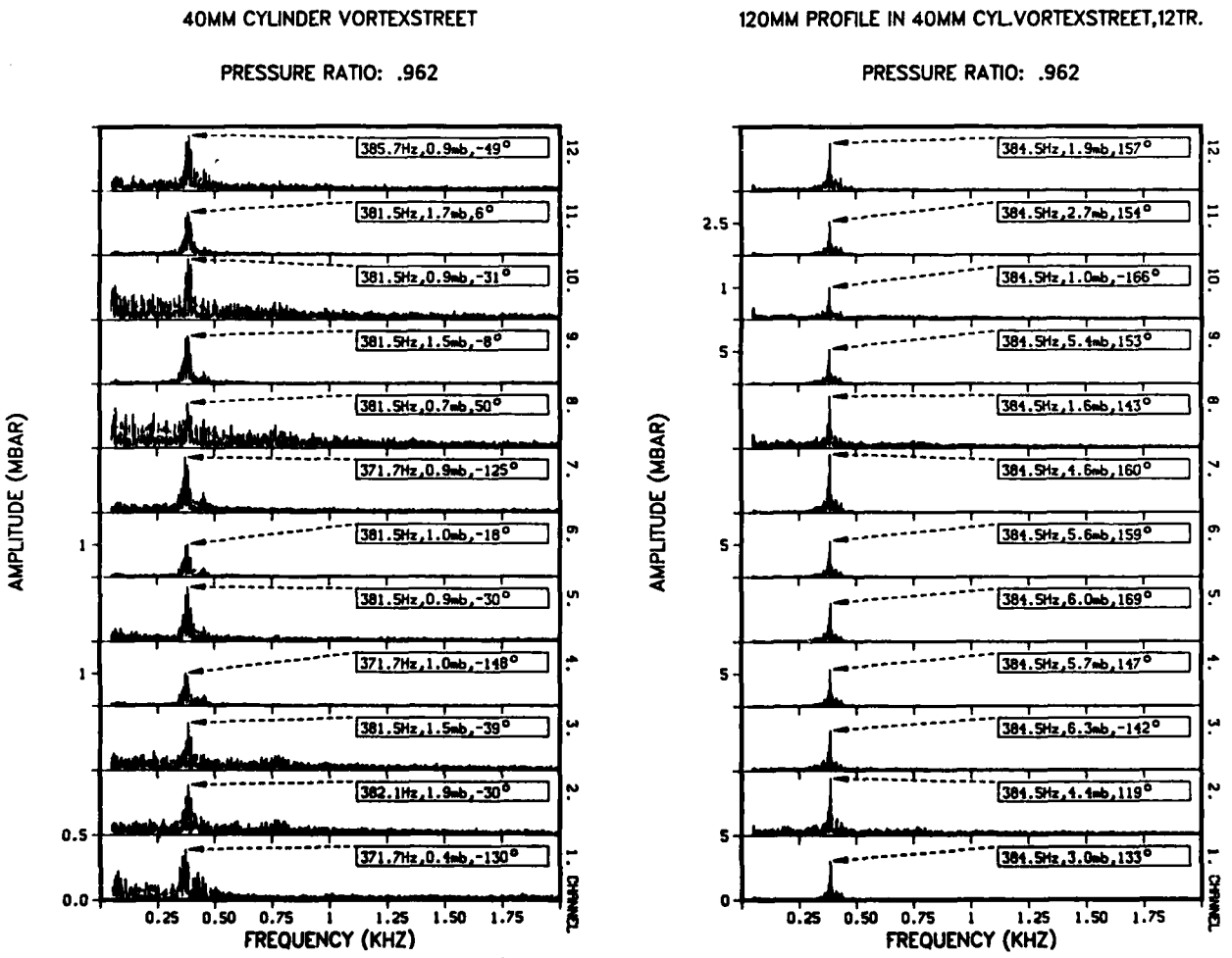


Figure 12a and 12b

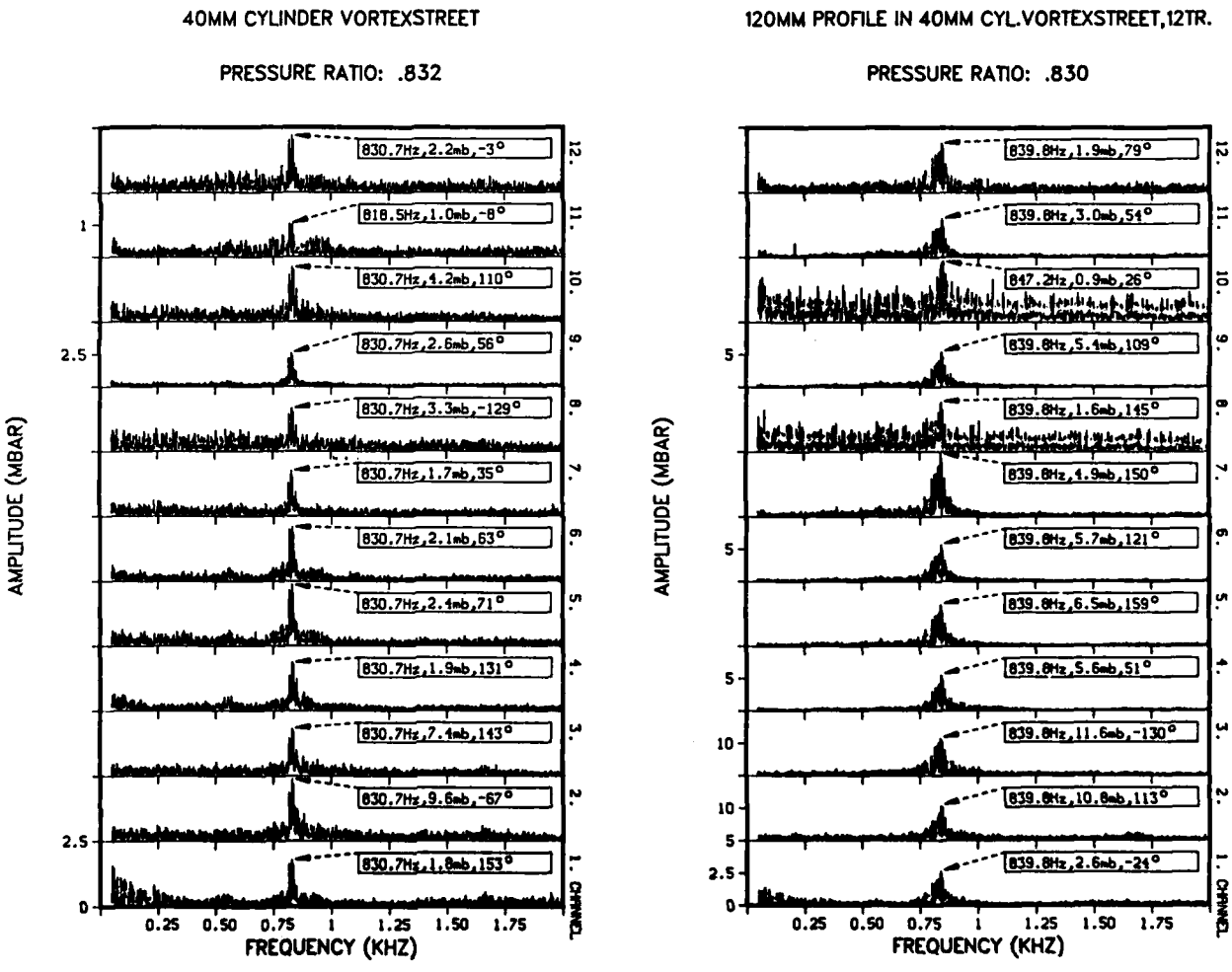


Figure 13a and 13b

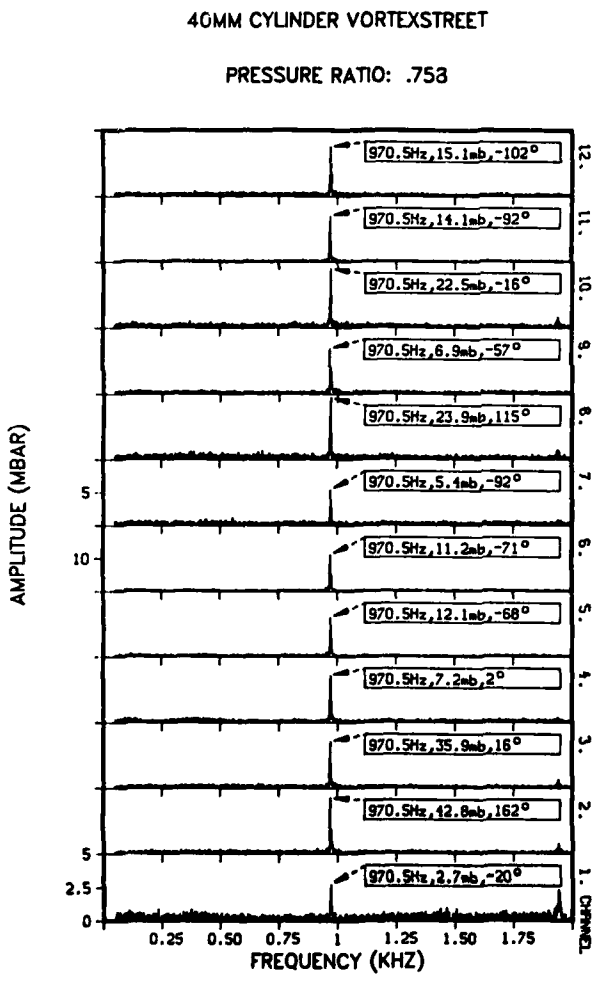


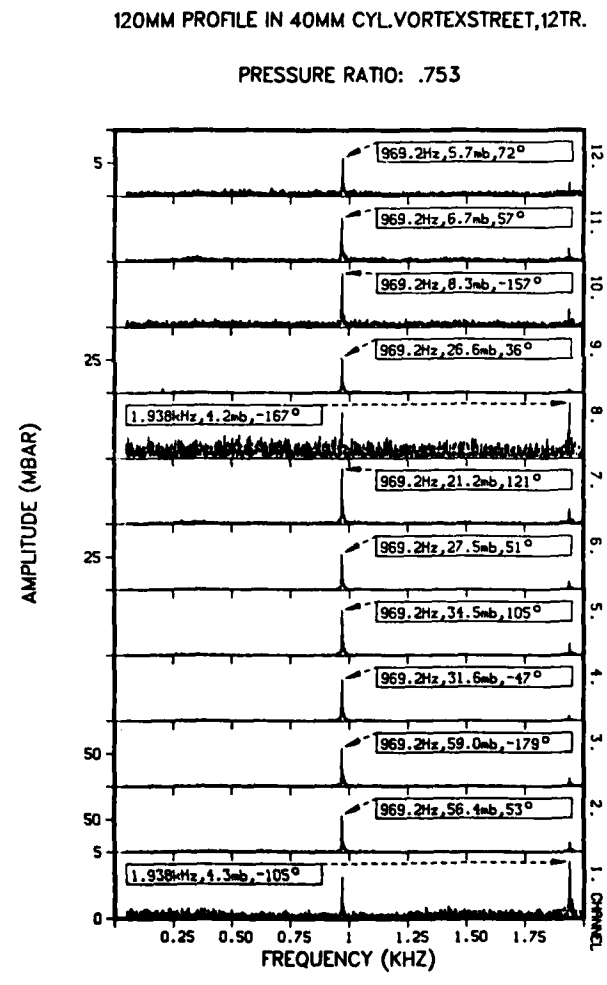


Figure 14a and 14b

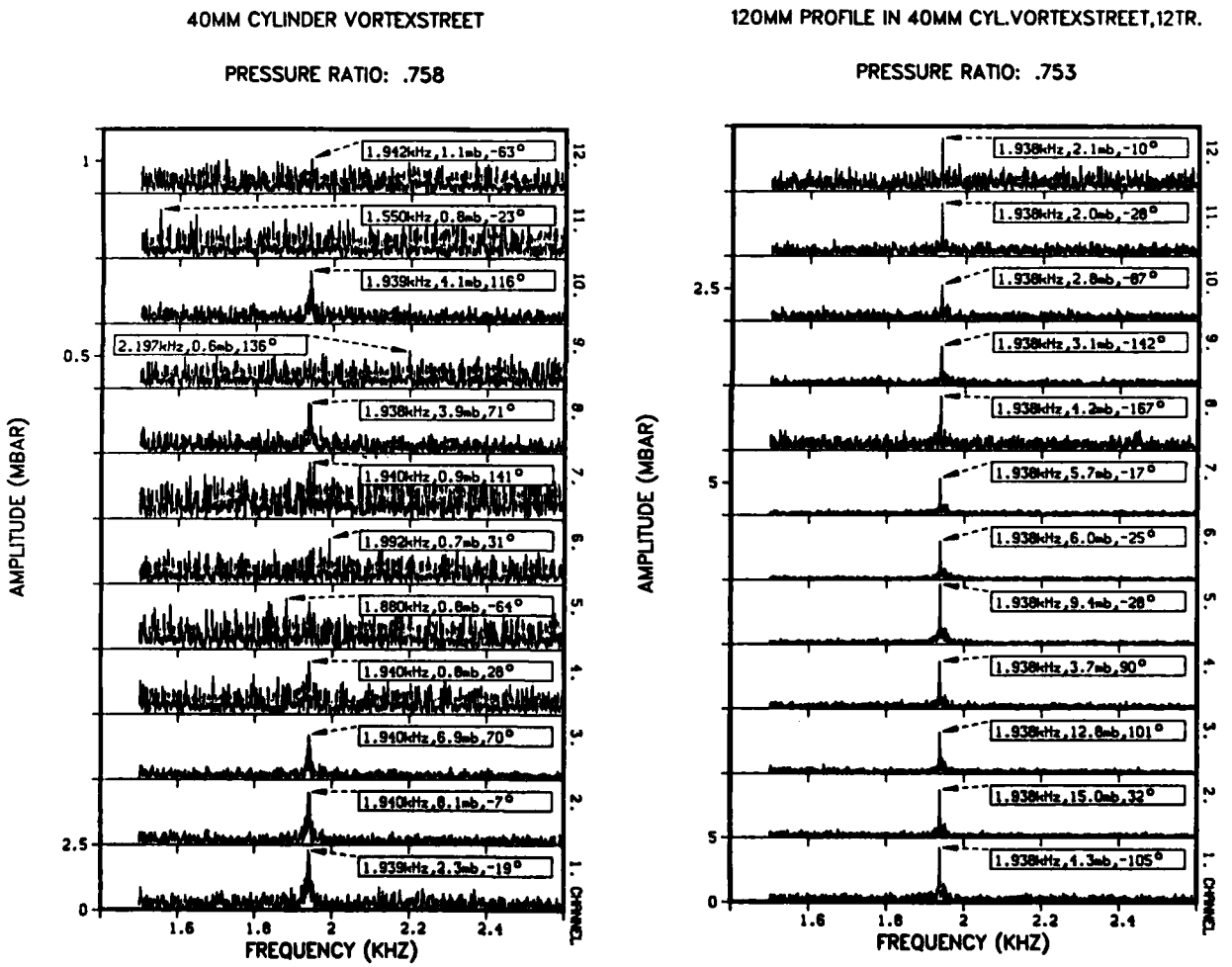


Figure 15a and 15b

Figure 16a, b and c: Vortex path under a Naca 0012 Profile at 100 [m/s]. Frames are taken from different vortices at subsequent phase angles.

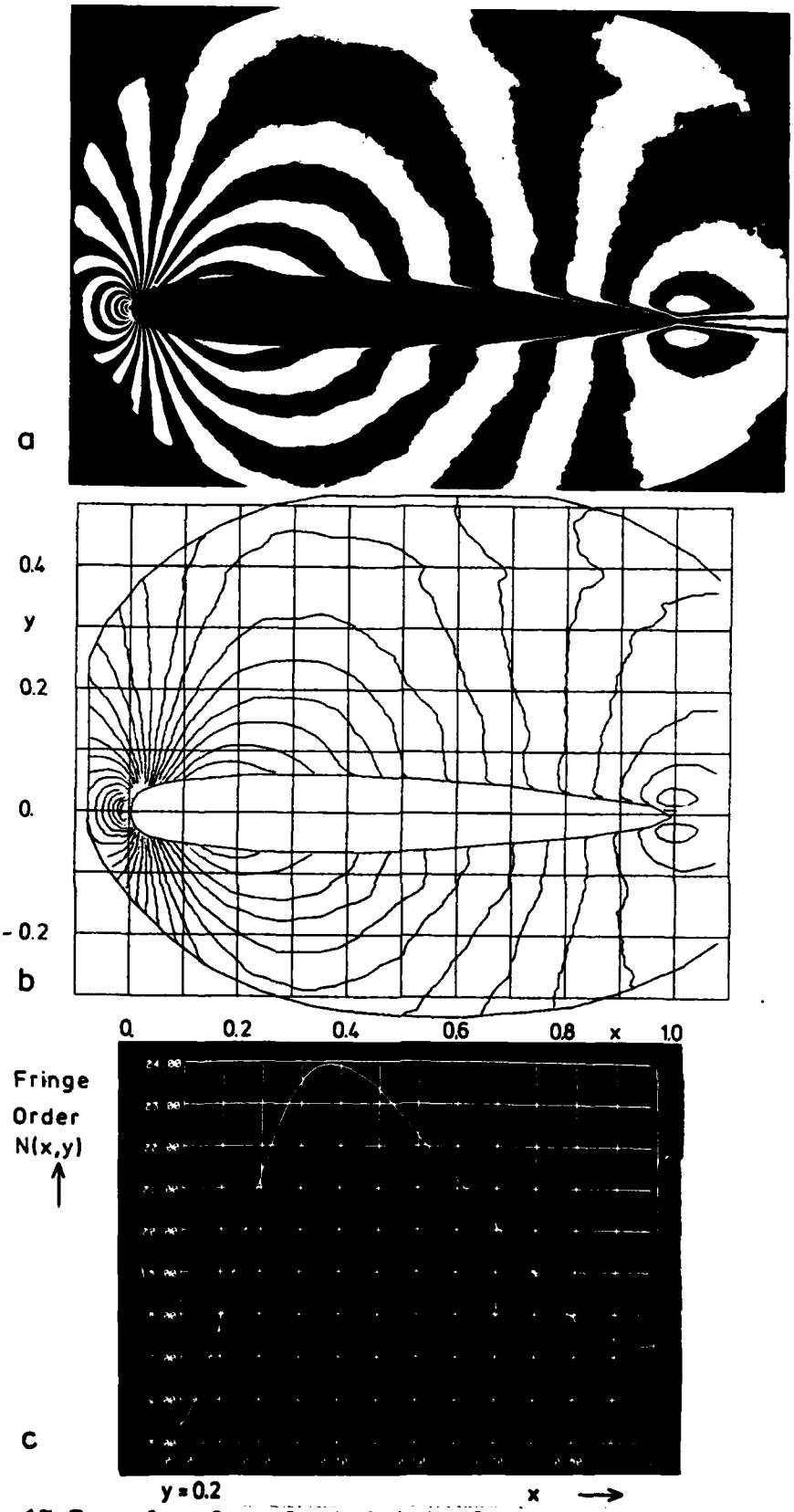


Figure 17 Example of evaluated interferograms

a) Photo of a profile flow interferogram
b) Plot of the segmented fringes of Fig. 17a after removal of the line disconnections. The mesh lines used for computing of the polynomial coefficients as well as the boundary lines of the testsection are included for illustration.
c) Density profiles plotted from the spline surface of the order number function of Fig. 17b along the x-direction at y=-0.2 The density is given in relative units (fringe numbers); high values represent low densities.

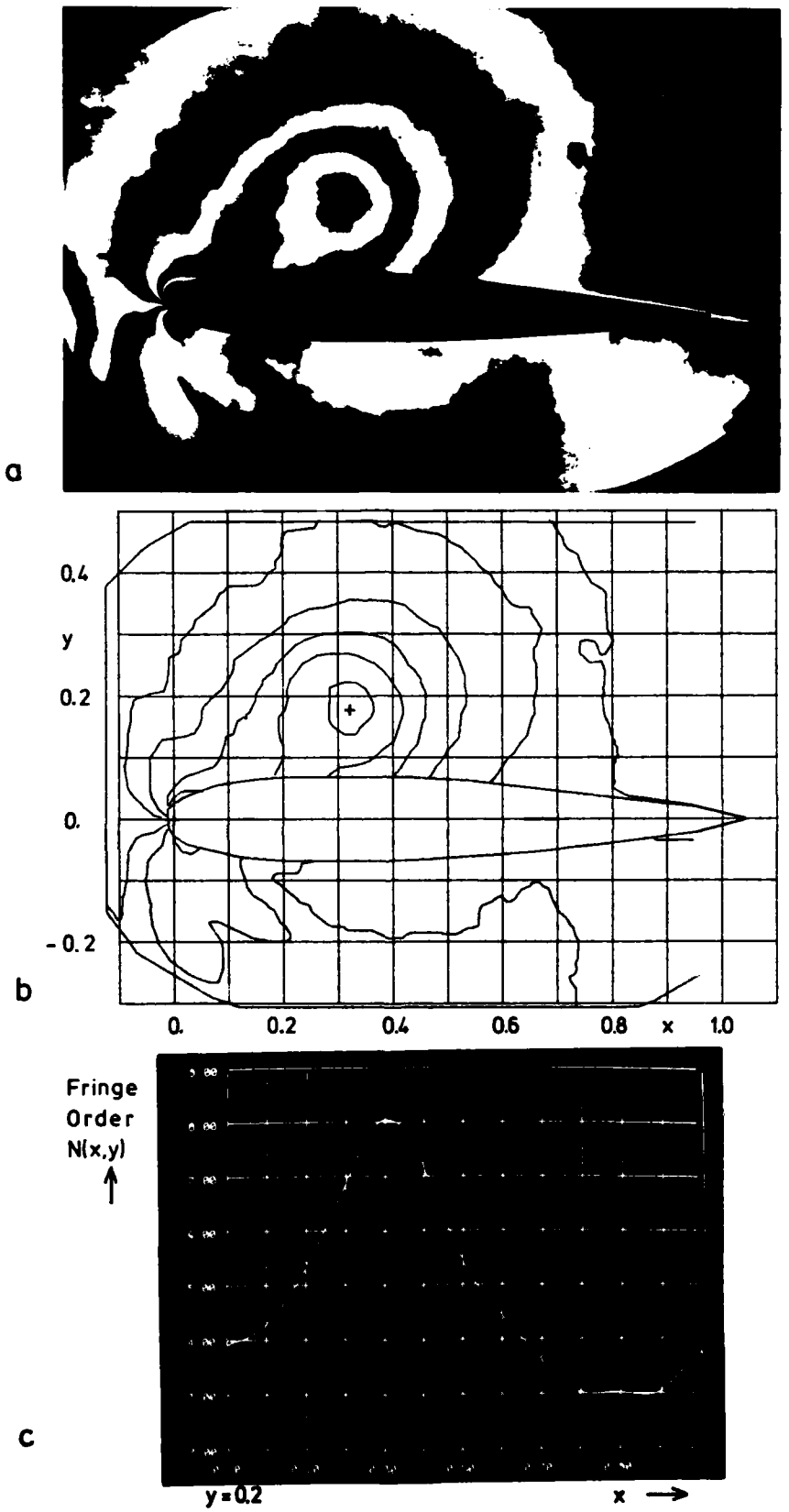


Figure 18 Example of evaluated interferograms
a) Photo of a profile flow interferogram with vortex
b) Plot of the segmented fringes of Fig. 18a after removal of the line disconnections. The position of the vortex core is at (x,y)=(0.32,0.18).
c) Density profiles plotted from the spline surface of the order number function of Fig. 18b along the x-direction at y=-0.2 The density is given in relative units (fringe numbers); high values represent low densities.

END

DATE
FILMED

7 83

DTIC